Development of a High-Resolution Time Conservative Finite Volume Method for Large Eddy Simulation

O. Aybay and L. He

School of Engineering, University of Durham, DH1 3LE Durham, UK

***Abstract*—A high-resolution time conservative two dimensional flow solver has been developed and validated for inviscid and viscous flows. The method is based on a multiblock structured grid. The space-time conservation element and solution element discretization scheme, second-order in space and time, is employed. Several cases with a wide range of flow conditions have been computed to verify the accuracy of method and demonstrate its effectiveness. An unsteady Euler solution is obtained for a forward facing step to demonstrate the shock capturing capability of the numerical scheme. The Navier-Stokes solver is validated with a cavity flow benchmark problem and the solution of the Navier-Stokes equations is accelerated with a direct flux-based multigrid method. A large eddy simulation (LES) of turbulence is performed for a spatially evolving mixing layer and compared with the results of a high-order scheme. The results using the present 2nd order scheme show high accuracy and high resolution, comparable those of high-order numerical schemes.**

***Index Terms*—CE/SE method, computational aero-acoustics, large eddy simulation, multigrid.**

I. Introduction

Computational aero-acoustics (CAA) is a tool that uses numerical simulations to predict flow induced sound. The modeling requirement of aeroacoustics problems is substantially different from traditional fluid dynamics problems. The acoustical signals are typically much smaller than those of mean flow variables and hence require much higher resolution and lower dissipations from computational methods. There are two approaches used to obtain accurate results for CAA problems. The first one employs standard computational fluid dynamics (CFD) methods with much finer meshes and the second one employs high-order numerical schemes.

Manuscript received October 30, 2007.

O. Aybay is with School of Engineering, University of Durham, DH1 3LE, Durham, UK (phone: +441913342412; fax: +441913342377; e-mail: orhan.aybay@durham.ac.uk).

L. He is with School of Engineering, University of Durham, DH1 3LE, Durham, UK (e-mail: li.he@durham.ac.uk).

For the standard second-order CFD schemes (e.g. central schemes, upwind schemes), they are generally too dissipative to adequately compute and simulate aeroacoustics problems [1]. The numerical schemes should resolve acoustic waves with low dissipation and low dispersion.

In the case of the high-order numerical schemes, they have been widely used for CAA applications. On the other hand, they attend to have difficulties in simulating regions with high gradients or discontinuities (e.g. at shock waves). The major drawbacks of the high-order schemes are the lack of a shock capturing property and difficulty to deal with the complex geometry. Spurious oscillations are frequently observed in the steep regions of the shock [2]. These non-physical oscillations of the flow variables can be dampened by employing low-order smoothing in the vicinity of large gradients. However, the smoothing would complicate and prevent the numerical scheme from being general. Furthermore, the smoothing would result in loss of accuracy [3]. The other difficult aspect of the high-order scheme is in application of the boundary conditions. The order of the schemes tends to be reduced on the boundaries which results in more complicated boundary condition treatments and again reduction of accuracy.

Therefore, there is a need for further development to address these issues associated with the standard second-order CFD schemes and the high-order schemes. The approach taken here is further advanced high resolution, low dissipation second-order scheme, aimed at solving complex unsteady aerodynamic and aeroacoustics problems with higher accuracy. The time conservative finite volume scheme, which is a good compromise between them, has been employed. This method is known as the space-time conservation element and solution element method, or the CE/SE method for short, originally proposed by Chang [4] at NASA Glenn Research Centre. In this method, space and time discretizations are coupled. The conservation of space-time flux is enforced over the surface of the control volume. On the other hand, the traditional methods focus only on the conservation of the spatial flux and they employ a separate discretization in space and in time. Furthermore, the flow variables and spatial derivative of the flow variables (i.e. gradients) are treated as unknowns. No knowledge of the waves or the direction of wave propagation is

required for the present scheme. Hence, the convective fluxes at the face of the control volume can be evaluated without using a Riemann solver. Another unique feature of the time conservative finite volume scheme is that simple but effective non-reflecting boundary conditions can be used due to the flux-based nature of the method. A detailed discussion of the CE/SE method based on coupled space and time discretization can be found in [4]. The CE/SE scheme was modified for a two-dimensional case using regular structured grid by Zhang and Yu [5]. A generalized structured grid extension for a single block can be found in Zhang *et al.* [6]. In this study, the numerical scheme given by Zhang *et al*. [6] is employed with some geometrical modifications.

The time conservative finite volume method is an explicit time-stepping scheme. The maximum permissible time step is restricted by the smallest grid cell due to the stability limitations. Particularly for viscous flows and highly stretched grid cells, time-step limitation results in a slow convergence. In order to accelerate the convergence of the Navier-Stokes solver the direct flux-based multigrid method is employed. Furthermore, the multiblock meshing is used for geometrically complex configurations. For simplicity, the number of grid points is taken as equal at both sides of a block interface. Hence, exchanging the physical quantities between the blocks becomes very straightforward.

In this study, Large Eddy Simulation (LES) is employed to simulate turbulent flows, since LES is well suited for detailed studies of complex unsteady flows and aerodynamic noise. Furthermore, LES is a good compromise between Reynolds-Averaged Navier-Stokes equations (RANS) and Direct Numerical Simulation (DNS).

For RANS calculations, the instantaneous flow quantities are represented by the sum of a mean value and a time-dependent fluctuating value. In order to compute the mean flow properties of turbulent flow, a time-averaged rate of momentum transfer (i.e. Reynolds stress tensor) need to be computed. Hence, the time averaging would result in loss of accuracy for detailed studies of complex unsteady flows. Furthermore, all scales of turbulence need to be modeled.

In the case of DNS, no turbulence model is required. However, DNS calculations are very expensive even at moderately high Reynolds number since all scales of turbulence have to be calculated directly.

In LES, all of the flow variables are decomposed into resolved (large) scales and subgrid (small) scales. The large scales are responsible for the most of momentum and energy transport. In contrast, the small scales are much weaker and also they have similar structure and characteristics. Hence, it is reasonable to directly compute the large scales and model the effect of the small ones. LES requires a higher grid resolution with respect to the RANS calculations. However, it is considerably cheaper than the DNS calculations [7].

II. Methodology

A. Flow Governing Equations and Subgrid-Scale Model

For compressible turbulent flows the Favre averaging together with the spatial filtering is a common approach since it does not alter the conservative form of the unfiltered governing equations. Furthermore, using any other filtering approach would introduce more complicated subgrid-scale terms in the governing equations due to additional correlation involving density fluctuations. Decomposition of the flow variables is given by

$$f = \widetilde{f} + f'' \tag{1}$$

where $\widetilde{f}$ represents the resolved part or a Favre-filtered and f'' the unresolved part of the flow variable. In fact, the governing equations are not explicitly filtered for the finite volume discretization method. The grid and the discretization errors are assumed to provide an implicit filter for the large eddies. The filtered variable is obtained as follows

$$\widetilde{f} = \frac{\overline{\rho f}}{\overline{\rho}} \tag{2}$$

LES equations can be obtained now by sorting all the above contributions and terms into the governing equations. The resulting equations describe the evolution of the resolved field and contain the subgrid-scale parts, which represent the effects of the instantaneous small-scale fluctuations on the resolved field. The Favre-filtered compressible Navier-Stokes equations are expressed as

$$\frac{\partial \overline{\rho}}{\partial t} + \frac{\partial \overline{\rho}\widetilde{u}_i}{\partial x_i} = 0 \tag{3}$$

$$\frac{\partial \overline{\rho}\tilde{u}_i}{\partial t} + \frac{\partial \overline{\rho}\tilde{u}_i\tilde{u}_j}{\partial x_j} + \frac{\partial \overline{p}}{\partial x_i} - \frac{\partial}{\partial x_j}(\hat{\sigma}_{ij} - \tau_{ij}) = 0 \tag{4}$$

$$\frac{\partial \overline{e}_t}{\partial t} + \frac{\partial \tilde{u}_i(\overline{e}_t + \overline{p})}{\partial x_i} - \frac{\partial}{\partial x_i}\tilde{u}_j(\hat{\sigma}_{ij} - \tau_{ij}) + \frac{\partial}{\partial x_i}(\hat{q}_i + Q_i) = 0 \tag{5}$$

where $\overline{e}_t$ is the total energy and defined as

$$\overline{e}_t = \frac{\overline{p}}{\gamma - 1} + \frac{1}{2}\overline{\rho}\widetilde{u}_i\widetilde{u}_i \tag{6}$$

$\hat{\sigma}_{ij}$, τ_{ij} , $\hat{q}_i$ and Q_i are resolved viscous stress tensor, subgrid-scale stress tensor, resolved heat flux and subgrid-scale heat flux, respectively.

The resolved scales can be solved directly by the Favre-filtered Navier-Stokes equations whereas to simulate momentum and energy transfer between the large and the subgrid scales. The subgrid-scale terms have to be modeled.

In this study due to its simplicity the classical Smagorinsky subgrid scale (SGS) model [8] is employed. The resolved viscous stress tensor is defined as:

$$\hat{\sigma}_{ij} = 2\tilde{\mu}(\tilde{S}_{ij} - \frac{1}{3}\tilde{S}_{kk}\delta_{ij}) \tag{7}$$

where δ_{ij} is the Kronecker delta and $\widetilde{S}_{ij}$ is the Favre-filtered strain rate tensor is defined as

$$\widetilde{S}_{ij} = \frac{1}{2}(\frac{\partial \widetilde{u}_j}{\partial x_i} + \frac{\partial \widetilde{u}_i}{\partial x_j}) \tag{8}$$

The subgrid-scale stress tensor is given by

$$\tau_{ij} = -\overline{\rho}(\widetilde{u_i u_j} - \tilde{u}_i \tilde{u}_j) \tag{9}$$

and is modeled as

$$\tau_{ij} = -2C_R\overline{\rho}\Delta^2\widetilde{S}_M(\widetilde{S}_{ij} - \frac{1}{3}\widetilde{S}_{kk}\delta_{ij}) + \frac{2}{3}C_I\overline{\rho}\Delta^2\widetilde{S}_M^2\delta_{ij} \tag{10}$$

where $\widetilde{S}_M = (2\widetilde{S}_{ij}\widetilde{S}_{ij})^{1/2}$, C_R and C_I are the Smagorinsky model constants and Δ is the filter width. The first term appearing in the right-hand side of relation (10) is the incompressible term in Smagorinsky's model [9] and the second term is the compressible correction known as Yoshizawa's expression [10].

The resolved heat flux is defined as

$$\hat{q}_i = -C_p\frac{\tilde{\mu}}{Pr}\frac{\partial \tilde{T}}{\partial x} \tag{11}$$

where C_P, $\tilde{\mu}$ and Pr are the specific heat a, the molecular viscosity and Prandtl number, respectively.

The subgrid-scale heat flux is given by

$$Q_i = -C_p\overline{\rho}(\widetilde{u_i T} - \tilde{u}_i\tilde{T}) \tag{12}$$

and the subgrid-scale heat flux is modeled using a temperature gradient approach as

$$Q_i = -C_p\frac{C_R\rho\Delta^2\widetilde{S}_M}{Pr_t}\frac{\partial \widetilde{T}}{\partial x_i} \tag{13}$$

In order to close the system of equations, the perfect gas relation and the Sutherland's law, respectively, are defined as

$$\overline{p} = \overline{\rho}R\tilde{T} \tag{14}$$

and

$$\tilde{\mu} = \mu_{ref}\left(\frac{\tilde{T}}{T_{ref}}\right)^{3/2}\frac{T_{ref}+S}{\tilde{T}+S} \tag{15}$$

where R is the ideal gas constant, T_{ref} and μ_{ref} are the reference temperature and the reference viscosity, respectively. S is chosen as $110K$.

The Navier-Stokes computations without turbulence terms can be carried out by replacing all filtered variables with their unfiltered forms and setting the subgrid-scale stress tensor and the subgrid-scale heat flux terms to be zero. Furthermore, for the inviscid Euler computations the viscous stress tensor set to zero.

B. Discretization

The time and space discretizations are coupled in the time conservative finite volume method. The computational domain is divided into quadrilateral grid cells, Fig. 1(a). The vertex of each grid cell is denoted by a circle symbol (i.e. A(i,j)), whereas the centroid of each grid cell is shown by a square symbol (i.e. C(i,j)). B_1(i,j), B_2(i,j), B_3(i,j) and B_4(i,j) are the midpoints of the cell-vertex.

Consider Fig. 1(b), the point denoted by the superscript $'$ is the point at time $n+1/2$ level. For time-marching from $t = t^0$ to $t = t^{n+1/2}$, the control volume is represented by the hexahedral A(i,j) A(i+1,j) A(i+1,j+1) A(i,j+1) A′(i,j) A′(i+1,j) A′(i+1,j+1) A′(i,j+1). Initially, the flow variables and the spatial derivatives of the flow variables are assumed to be known at the vertex of each grid cells (i.e. A(i,j)) at time level $t = t^0$. Then, the conservation of space-time flux is enforced over the surface of the control volume to calculate the flow variables associated with point C′(i,j) at time level $t = t^{n+1/2}$. A central difference approach is employed to calculate the spatial derivative of the flow variables.

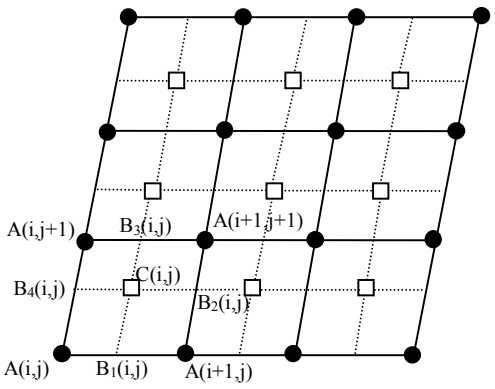

(a) 2-D structured grid

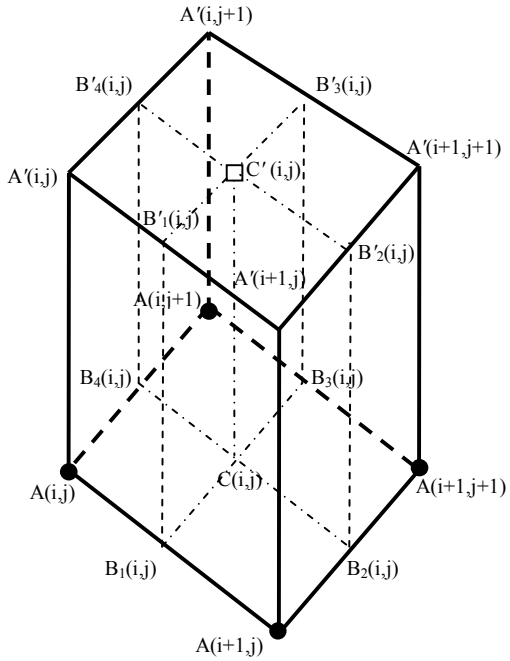

(b) Control volume

Fig. 1 Structured grid and control volume for the 2-D Euler/Navier-Stokes solver for time-marching from $t = t^0$ to $t = t^{n+1/2}$

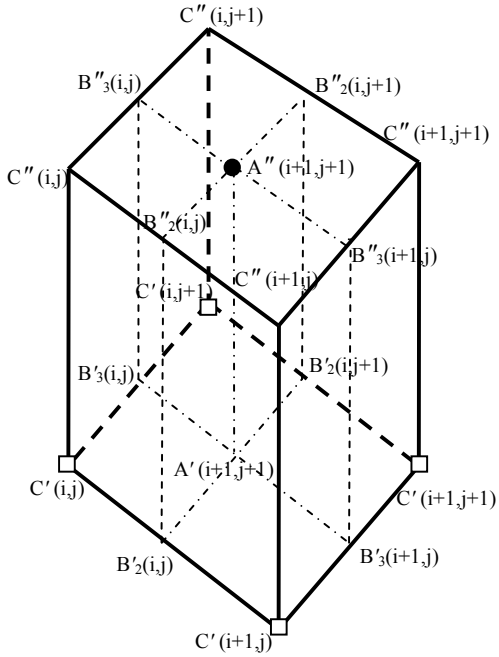

(b) Control volume

Fig. 2 Structured grid and control volume for the 2-D Euler/Navier-Stokes solver for time-marching from $t = t^{n+1/2}$ to $t = t^{n+1}$

For time-marching from $t = t^{n+1/2}$ to $t = t^{n+1}$, consider Fig. 2(a) and Fig. 2(b), the point represented by the superscript ″ is the point at time $n+1$ level. Similarly, at time level $t = t^{n+1}$ to evaluate the flow variables and the gradients associated with point A″(i+1,j+1) the same procedure repeated for the control volume C′(i,j) C′(i+1,j) C′(i+1,j+1) C′(i,j+1) C″(i,j) C″(i+1,j) C″(i+1,j+1) C″(i,j+1). Thus, the numerical scheme alternates between the cell-vertex and the cell-centre of the grid cells.

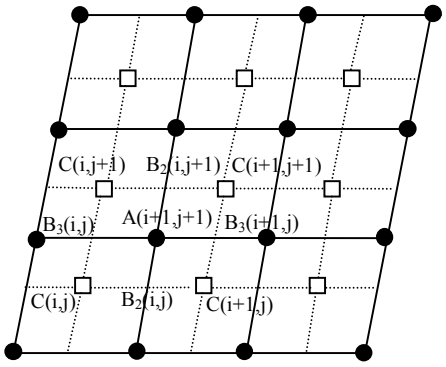

(a) 2-D structured grid

The main advantage of this modification is apparent that all of the control volume is left inside the physical domain at the boundary. Hence, there is no need to generate dummy cells outside the physical domain and this leads to decreased discretization error in comparison to the numerical scheme given by Zhang *et al.* [6].

The conservative variables and the convective fluxes are assumed to be linear whereas the viscous fluxes are assumed to be constant in the control volume. The conservative variables and the convective fluxes are discretize by the first order Taylor series expansion.

C. Direct Flux-Based Multigrid Method

In order to reduce the run-time requirement of the simulations for the viscous flows and the highly stretched grid cells, a direct flux-based multigrid method at two-level proposed by He [11] is employed as a convergence acceleration technique in this study.

For the two-level time integration method the solution is marched first on the fine grid and then on a coarser one. Hence, the overall time step is much larger than the one level temporal change and the accuracy of the solution is controlled by the fine grid. The temporal change of the flow variables on the fine grid is given by

$$(U^{n+1} - U^n)_f = \Delta t_f \frac{R_f}{\Delta V_f} + \Delta t_c \frac{R_c}{\Delta V_c} \tag{16}$$

where the subscript *f* and *c* denote the fine and coarse grid, respectively. Δt and *R* are the permissible time step and the net flux for the finite volume on the corresponding grid, respectively. Implementation of the direct flux-based multigrid method is much easier and numerically cheaper than the conventional one. A detailed discussion of the two-level multigrid method can be found in [11].

III. Results and Discussion

A. Flow over a Forward Facing Step

A supersonic flow over a forward facing step problem is solved to demonstrate the robustness of the present numerical scheme. This benchmark problem is the same as the one studied by Woodward and Colella [12]. It was also used by Giannakouros and Karniadakis [13]. The physical domain is first divided into three multiblocks. The present computations are carried out by using a 2-D multiblock Euler solver. The computational domain is 3.0 m × 1.0 m. Uniform structured mesh is used with Δx = 0.0125 m and Δy = 0.01 m grid spacing in the *x* and *y* directions, respectively. The free stream Mach number is 3.0, the stagnation pressure is 10^5 Pa and the stagnation temperature is 300 K. These flow conditions are imposed on the left-hand boundary as the supersonic inlet boundary condition. The upper and the lower boundaries are an inviscid wall, where a slip boundary condition is imposed. Lastly, the supersonic outflow boundary condition is applied on the right-hand boundary.

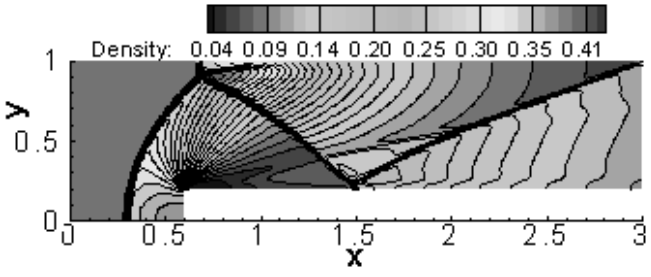

(a) t = 2.8 × 10^{-2} s

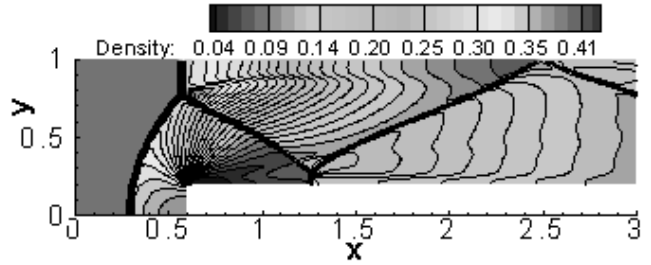

(b) t = 4.0 × 10^{-2} s

Fig. 3 Density contours with 30 levels

Calculated density profiles with 30 contours at t = 2.8 × 10^{-2} s and t = 4.0 × 10^{-2} s are shown in Fig. 3(a) and Fig. 3(b), respectively. The Mach stem in the lower wall, expansion fan at the corner of the step and the interaction between the reflected shocks with rarefaction waves are accurately calculated with high resolution. According to Woodward and Colella [12], without applying special numerical treatment at the corner of the step, calculations would be affected by large numerical errors. However, the present calculations are carried out without employing any special treatment at the corner of the step and no numerical oscillations are detected around a shock wave

B. Driven Cavity Flow

The driven cavity flow in a square cavity is used as a validation case for a Navier-Stokes solver. Direct flux-based multigrid method is employed at two-level in order to reduce to run-time requirement of the simulation. Although the cavity geometry is simple, this benchmark problem displays several complex flow phenomena, such as corner separations, longitudinal vortices and interaction between vortices depending on the Reynolds number.

The flow conditions are a free stream Mach number of 0.1, Reynolds number of 1000 based on the cavity length, stagnation pressure of 10^5 Pa and stagnation temperature of 300 K. The nonuniform mesh density is 129 × 129 in the *x* and *y* directions, respectively. The upper boundary is moving at a speed of free stream Mach number and the other three boundaries are stationary (i.e. viscous) walls where a no-slip boundary condition is imposed.

A primary vortex inside the cavity and two smaller reverse-rotating vortices at both corners of the bottom wall can be observed with Mach number contours and the streamlines in Fig. 4. For the two-level multigrid method, *u*-velocity profile along the vertical line and *v*-velocity profile along the horizontal line through the geometric centre of the cavity are compared with Ghia's results [14] in Fig 5 and Fig. 6, respectively. The results using the present 2nd order scheme are in good agreement with Ghia's results [14], showing high accuracy.

The comparison of residual history for the driven cavity flow is presented in Fig. 7. The comparison shows the improvement by employing a multigrid method with respect to a single grid calculation. The steady state is reached when the residual dropped approximately 5.5 - 6 orders of magnitude and due to the use of the larger time step the steady state can be quickly reached in multigrid solutions without losing any significant accuracy.

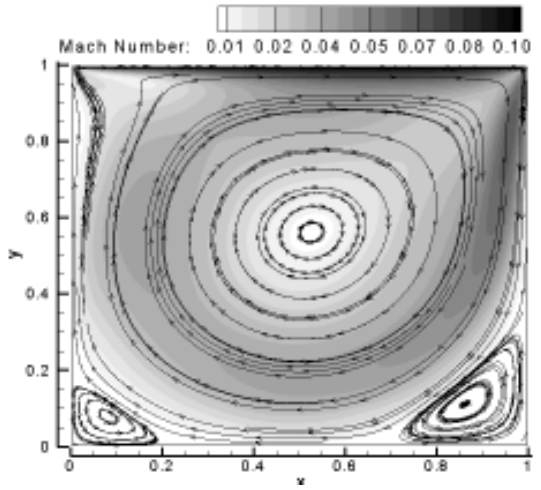

Fig. 4 Mach number contours and streamlines

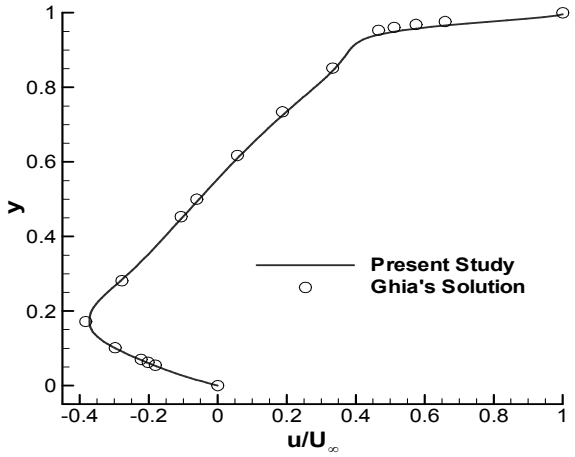

Fig. 5 *u*-velocity profile along the vertical line through the geometric centre of cavity

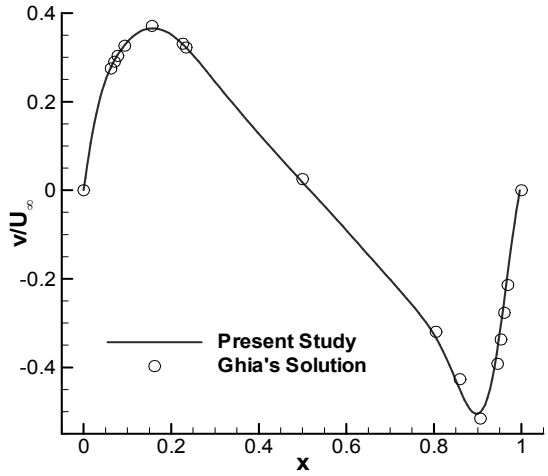

Fig. 6 *v*-velocity profile along the horizontal line through the geometric centre of cavity

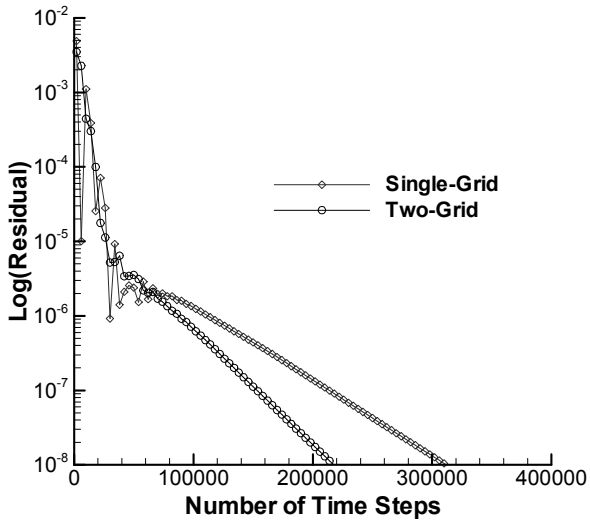

Fig. 7 Comparison of residual history of momentum in *x* direction for laminar flow over a flat plate

C. Large Eddy Simulation of Mixing Layer

A two-dimensional spatially evolving mixing layer problem is solved. This test case was also studied by Uzun [8] and Bogey [15]. In this study, a smaller computational domain (i.e. no sponge region) is used due to the present effective non-reflecting boundary conditions. The in-flow hyperbolic tangent velocity profile and the transverse velocity with random perturbations are, respectively, expressed as

$$u(y) = \frac{U_1 + U_2}{2} + \frac{U_2 - U_1}{2} \tanh\left(\frac{2y}{\delta_{\omega 0}}\right) \tag{17}$$

where U_1 = 50 m/s and U_2 = 100 m/s are the lower and upper velocities, respectively. $\delta_{\omega 0} = 1.6 \times 10^{-3}$ m is the initial vorticity thickness. The transverse velocity with a random perturbation is given by:

$$v(y) = \in \alpha\left(\frac{U_1 + U_2}{2}\right)\exp\left(\frac{-y^2}{\Delta y_0^2}\right) \tag{18}$$

where α = 0.0045, Δy_0 is the minimum grid spacing in the *y* direction and $\in$ is a random number between -1 and 1. The non-reflecting boundary conditions are imposed at the upper and the lower boundaries. The convective Mach number which measures the intrinsic compressibility of a mixing layer [16] is defined as:

$$M_c = \frac{U_2 - U_1}{2c_\infty} = 0.074 \tag{19}$$

where c_∞ is the free stream speed of sound. The Reynolds number based on the initial vorticity thickness ($\delta_{\omega 0}$) and velocity difference is given by:

$$\mathrm{Re}_{\omega} = \frac{\delta_{\omega 0}(U_2 - U_1)}{\nu} = 5333 \tag{20}$$

The mesh density is 625 × 301 in the x and y directions, respectively. The computational domain lies between $0 \le x \le 0.4$ m and -0.16 m $\le y \le 0.16$ m . The mesh is uniform in the streamwise direction whereas in the transverse direction exponential grid stretching is applied. The minimum grid spacing is about $0.16\delta_{\omega 0}$ at $y = 0$ and the maximum grid spacing around the lower and upper boundaries is $3.0\delta_{\omega 0}$.

In Fig. 8, instantaneous vorticity contours are shown and vortex pairing at different locations can be observed. The vorticity thickness evaluation is shown in Fig. 9. After the initial transients, the vorticity thickness grows linearly. The spreading rate parameter is given by [17]:

$$S = \frac{0.5(U_1 + U_2)}{U_2 - U_1}\frac{\partial \delta_{\omega}(x)}{\partial x} = 0.09 \tag{21}$$

The range of reported experimental results for the parameter S is from $S \approx 0.06$ to $S \approx 0.11$ [17]. The parameter S predicted by Smagorinsky model is within the range of experimental values. The normalized Reynolds stresses are defined as:

$$\sigma_{xx} = \frac{\langle u'u' \rangle}{(U_2 - U_1)^2},\ \sigma_{yy} = \frac{\langle v'v' \rangle}{(U_2 - U_1)^2} \tag{22}$$

where $\langle\rangle$ denotes time-averaging. In Fig. 10 and Fig. 11 the turbulence intensities are compared with Uzun's normalized Reynolds stress results [8] at different locations. For comparison the transversal direction is non-dimensionalized by the vorticity thickness $\delta_{\omega}(x)$. The calculated turbulence intensities are in good agreement with those using the 6th order tri-diagonal compact scheme of Uzun [8] whereas the present scheme is just 2nd order in space and time.

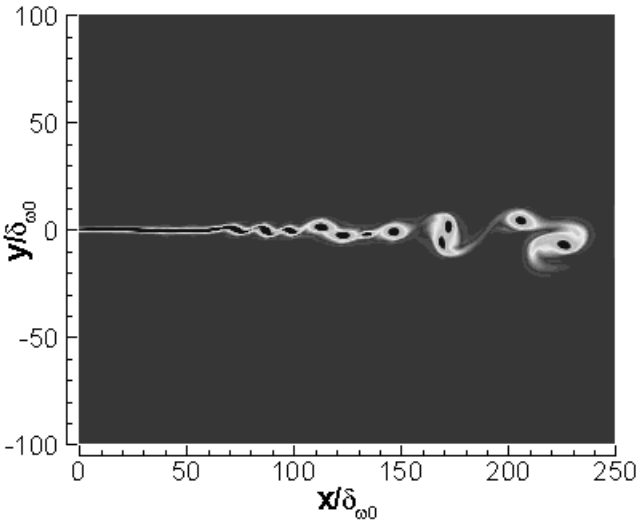

Fig. 8 Instantaneous vorticity contours

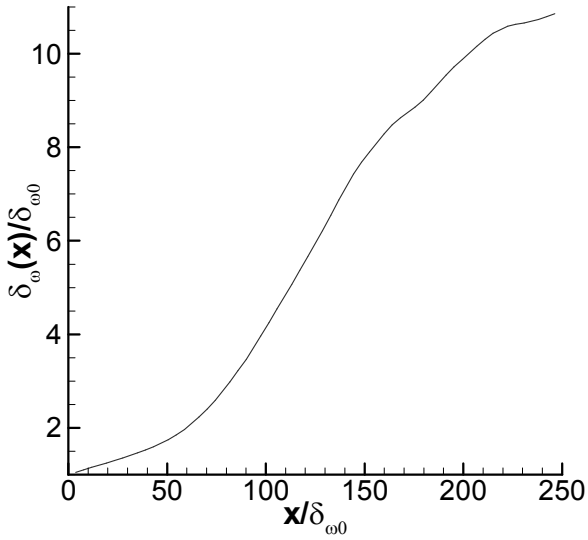

Fig. 9 Vorticity thickness growth in the mixing layer

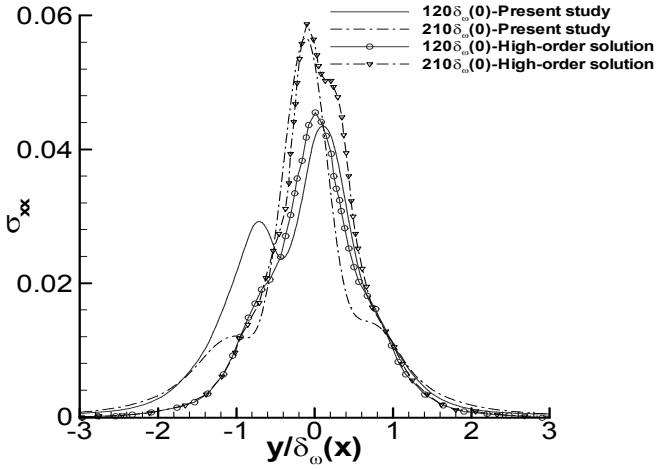

Fig. 10 Normalized Reynolds normal stress σ_{xx} profiles

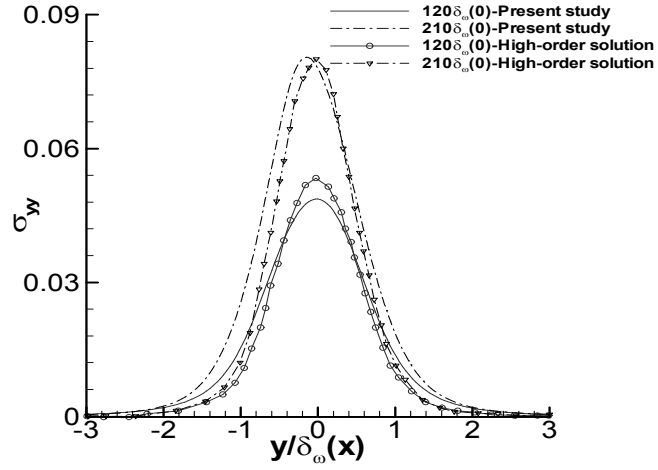

Fig. 11 Normalized Reynolds normal stress σ_{yy} profiles

IV. Concluding Remarks

This paper describes the first-known validation of a direct flux-based multigrid acceleration method for a Navier-Stokes solver employing the time conservative finite volume method.

Flow over a forward facing step test case is solved to demonstrate the robustness of the time conservative scheme. High accuracy and high resolution results have been achieved with low dissipation and low dispersion errors. No numerical oscillations are observable in the steep region around a shock wave. Furthermore, the simple but effective non-reflecting boundary conditions can be used with the present scheme.

The driven cavity flow in a square cavity is solved to validate the Navier-Stokes solver. The direct flux-based multigrid method is coupled with the scheme to effectively accelerate the convergence of the steady flow solution.

LES of turbulent flow is performed for a spatially evolving mixing layer and compared with the results from a sixth-order tri-diagonal compact scheme. The subgrid scale turbulence fluctuations are modelled with the Smagorinsky SGS model. The results are in good agreement with those from a high-order numerical scheme.

The second-order time conservative finite volume method is less dissipative than the other second-order numerical schemes and gives comparable results with high-order numerical schemes. High accuracy and high resolution coupled with non-oscillatory property of the present 2nd order scheme make it a good candidate for complex unsteady flows and computational aero-acoustics (CAA) applications.

Acknowledgment

The authors wish to thank Dr. Ali Uzun at the Florida State University for many helpful discussions.

References

[1] C. Y. Loh, "Nonlinear Aeroacoustics Computations by the CE/SE method," NASA CR-2003-212388, 2003.

[2] C. K. W. Tam and J. C. Webb, "Dispersion-Relation-Preserving Finite Difference Schemes for Computational Acoustics," *Journal of Computational Physics,* vol. 107, Aug. 1993, pp. 262-282.

[3] E. Envia, A. G. Wilson and D. L. Huff, "Fan Noise: A Challenge to CAA," *International Journal of Computational Fluid Dynamics,* vol. 18, no. 6, Aug. 2004, pp. 471-480.

[4] S. C. Chang, "The Method of Space-Time Conservation and Solution Element – A New Approach for Solving the Navier-Stokes and Euler Equations," *Journal of Computational Physics,* vol. 119, July 1995, pp. 295-324.

[5] Z. C. Zhang and S. T. Yu, "Shock Capturing without Riemann Solver – A Modified Space-Time CE/SE method for Conservation Laws," AIAA 99-0904, 1999.

[6] Z. C. Zhang, S. T. Yu and S. C. Chang, "A Space-Time Conservation Element and Solution Element Method for Solving the Two and Three Dimensional Unsteady Euler Equations using Quadrilateral and Hexahedral Meshes," *Journal of Computational Physics,* vol. 175, Jan. 2002, pp. 168-199.

[7] J. Blazek, *Computational Fluid Dynamics: Principles and Applications*, Elsevier, 2005, ch. 3.

[8] A. Uzun, *3-D Large Eddy Simulation for Jet Aeroacoustics* PhD thesis, Purdue University, USA, Dec. 2003.

[9] Smagorinsky, J. S., "General Circulation Experiments with the Primitive Equations," *Monthly Weather Review*, Vol. 91, No.3, March 1963, pp. 99-165.

[10] Yoshizawa, A., "Statistical Theory for Compressible Turbulent Shear Flows, with Application to Subgrid Modeling," *Physics of Fluids*, Vol. 29, No. 7, July 1986, pp. 2152-2164.

[11] L. He and J. D. Denton, "Three-Dimensional Time-Marching Inviscid and Viscous Solutions for Unsteady Flows Around Vibrating Blades," *Journal of Turbomachinery,* vol. 116, July. 1994, pp. 469-476.

[12] P. Woodward and P. Colella, "The Numerical Simulation of Two-Dimensional Fluid Flow with Strong Shock," *Journal of Computational Physics,* vol. 54, April 1984, pp. 115-173.

[13] J. Giannakouros and G. E. Karniadakis, "A Spectral Element-FCT Method for the Compressible Euler Equations," *Journal of Computational Physics,* vol. 115, Dec. 1994, pp. 65-85.

[14] U. Ghia, K. N. Ghia and C. T. Shin, "High-Re Solutions for Incompressible Flow Using the Navier-Stokes Equations and a Multigrid Method," *Journal of Computational Physics,* vol. 48, 1982, pp. 387-411.

[15] C. Bogey, *Calcul Direc du Bruit Aérodynamique et Validation de Modèles Acoustiques Hybrides* PhD thesis , Laboratoire de Mécanique des Fluides at d'Acoustique, École CEntrale de Lyon, France, April 2000.

[16] C. Le Ribault, "Large Eddy Simulation of Compressible Mixing Layers," *International Journal of Computational Fluid Dynamics,* vol. 1, no. 1, 2005, pp. 87-111.

[17] S. B. Pope, *Turbulent Flows*, Cambridge University Press, 2000, ch. 5.